# Three-dimensional Marangoni cell in self-induced evaporating cooling unveiled by digital holographic microscopy

Christophe Minetti and Cosimo Buffone*

*Microgravity Research Centre, Université libre de Bruxelles, Avenue F. D. Roosevelt 50, 1050 Bruxelles, Belgium*

(Received 24 June 2013; revised manuscript received 9 September 2013; published 13 January 2014)

A digital holographic microscope has been used to trace the trajectory of a tracer particle inside the liquid phase of an evaporating meniscus formed at the mouth of a 1-mm$^2$ borosilicate tube filled with ethanol. The Marangoni flow cells are generated by the self-induced differential evaporating cooling along the meniscus interface that creates gradients of surface tension which drive the convection. The competition between surface tension and gravity forces along the curved meniscus interface disrupts the symmetry due to surface tension alone. This distorts the shape of the toroidal Marangoni vortex. Thermocapillary instabilities of the evaporating meniscus are reported by analyzing the trajectories of the tracer particle. It is found that the trajectory of the tracer particle makes different three-dimensional loops and every four loops it returns to the first loop. By analyzing several loops it was found that the characteristic frequency of the periodic oscillatory motion is around 0.125 Hz.

DOI: 10.1103/PhysRevE.89.013007 PACS number(s): 47.55.pf

## I. INTRODUCTION

Surface tension plays an important role in many industrial applications from oil extraction to combustion, to boiling, evaporation and condensation, to crystal growth, to heat pipes, just to mention but a few. Surface tension is really important in defining the interface at microscale as demonstrated by Levich and Krylov [1]. For such problems a dimensionless number is introduced, which represents the ratio $\frac{\mathrm{Ma}}{\mathrm{Ra}} = \frac{\sigma}{\rho g \beta}\frac{1}{R^2}$, where Ma and Ra are the Marangoni and Rayleigh numbers, respectively, $\sigma$ is the surface tension, $\rho$ liquid density, g gravitational acceleration, $\beta$ the volumetric expansion coefficient, and $R$ the characteristic length); when introducing the capillary length $l_c = \sqrt{\frac{\sigma}{\rho g}}$, the ratio becomes $\frac{\mathrm{Ma}}{\mathrm{Ra}} = \frac{1}{\beta}(\frac{l_c}{R})^2$. Therefore, for $R < l_c$ (thin liquid films) Benard-Marangoni convection dominates, whereas for $R > l_c$ (thick liquid films) Rayleigh-Benard convection dominates as reported in Zeytounian [2]. For the present case we have $R = 1$ mm and $l_c = 1.7$ mm; therefore thermocapillary forces dominate. That said, Buffone *et al.* [3] reported significant distortion of the Marangoni cells because of the gravity forces in a diametrical vertical section of the horizontal positioned tube. Buffone *et al.* [4] reported oscillations in the Marangoni vortex as well as in the meniscus interface. The Marangoni number is an important dimensionless number describing surface tension dominated phenomena and is the ratio between surface tension and viscous forces. The role of surface tension was first recognized by Pearson [5], while the Marangoni number was first introduced by Scriven and Sternling [6].

The differential evaporative cooling effect along the curved meniscus interface has been found to be responsible for the differences in temperature and consequently surface tension that drives the Marangoni convection. Wang *et al.* [7] postulate a different explanation related to the diffusion of vapor in still air above the meniscus. In particular they argue that the evaporation rate is higher at the meniscus wedge than at the center; this is because the meniscus wedge is closer to the tube mouth than the center and therefore the vapor transports more efficiently at the wedge.

When a liquid meniscus is formed as in evaporation, condensation, or boiling, there are three important regions, namely, macroregion, microregion, and adsorbed layer. Much work was done in the 1970s by Wayner and co-workers in understanding the mechanism involved in the heat and mass transfer from evaporating thin liquid films (Potash and Wayner [8], Potash and Wayner [9], Preiss and Wayner [10], Wayner *et al.* [11]). The subject was, however, still not fully understood as was demonstrated by numerous other works that have appeared in the area in the 1990s (see Mirzamoghadam and Catton [12], Swanson and Herdt [13], DasGupta *et al.* [14], Wayner [15], Reyes and Wayner [16], Khrustalev and Faghri [17], Schonberg *et al.* [18]). The main unsolved issue of these aforementioned authors is the hydrodynamics in the liquid phase of the meniscus. This has become possible recently because of the use of powerful tools such as particle tracking at microscale and microparticle image velocimetry. More recently it has been clearly experimentally demonstrated (Sartre *et al.* [19], Hohmann and Stephan [20], and Buffone and Sefiane [21]) that the evaporation peaks indeed in the microregion (as was postulated by earlier work) which is typically a few micrometers in length. In the present case the higher evaporation at the meniscus wedge (where the microregion is found) with respect to the meniscus center creates temperature gradients which generate surface tension gradients that in turn drive the Marangoni convection under investigation.

One of the present authors reported in several works the self-induced Marangoni convection of volatile liquids (alcohols) evaporating inside capillary tubes with size ranging from 600 to 1630 microns. The tubes were placed horizontally (Buffone and Sefiane [22]) but also vertically (Buffone and Sefiane [23]) and the convection was characterized by $\mu$-particle image velocimetry ($\mu$-PIV). $\mu$-PIV is a powerful experimental technique that allows mapping the velocity field at microscale by using tracer particles that scatter coherent light from a laser source; this scattered light is recorded on a charge-coupled device (CCD) camera for subsequent correlation using specialized statistical software (Markus *et al.* [24]). Temperature measurements close to the meniscus

*Corresponding author: cbuffone@ulb.ac.be

 

interface were also carried out (Buffone and Sefiane [25]) for a variety of liquids and tube sizes by using infrared thermography. The temperature measurements clearly showed a lower temperature at the meniscus wedge than at the meniscus center. This is due to larger evaporation rate at the meniscus wedge than in the center. These studies clearly demonstrated that thermocapillary convection is self-induced by the differential evaporation rate along the meniscus interface.

In some applications such as crystal growth (Schwabe [26]) it is important that the final product is free of defects which are originated from disuniformities in the phases. For this reason it is important that there are no distortions in the phases due to the competition of surface tension and gravity as those reported in Buffone *et al*. [3]. It is therefore mandatory that proper investigation is carried out to assess the minimum size below which there are no distortions in the flow field. Chamarthy *et al*. [27] reported interesting $\mu$-PIV results of methanol evaporating inside capillary tubes of 75, 200, and 400 $\mu$m. They improved the $\mu$-PIV experiments by being able to do several horizontal cross sections at different heights with respect to the diametrical section of the tube, and also vertical diametrical sections. They showed clearly that for the 75-$\mu$m tube there is no influence of gravity on the convection pattern; whereas for the 200- and 400-$\mu$m tubes they confirm that buoyancy forces distort the otherwise symmetrical flow pattern.

Instabilities of the toroidal Marangoni vortex have been recently reported in Pan *et al*. [28]. The authors showed that the Marangoni flow in a concave meniscus is always symmetrical to the tube axis whereas that on a convex meniscus loses symmetry with only one vortex occupying the whole channel. Additionally, it was found that the Marangoni flow from the meniscus wedge to its center is not as stable as the opposite flow.

One of the major limitations of previous work (Buffone *et al*. [3,4] and Buffone and Sefiane [22]) is the fact that it was not possible to follow the three-dimensional (3D) trajectory of the seeding particles. This was due to the very narrow depth of focus (from 6 to 27 microns) of the standard microscope used which did not allow seeing the particles in their 3D motion. In the present work a digital holographic microscope (DHM) has been used which can see $\pm$500 microns above and below the nominal optical median section of the tube. The use of the DHM allowed following single particles and unveiling the 3D periodic motion.

## II. EXPERIMENTAL SETUP

Over the last 10 years, digital holography has attracted a lot of attention in the scientific community and particularly in the field of microscopy. Classical microscopy suffers from a very small depth of focus due to the high numerical apertures (NAs) of the microscope lenses and the high magnification. Confocal microscopes strongly enlarge the depth of field of classical microscopes but are not adequate for nonstatic phenomena as it requires scanning point-by-point in the three directions. DHM overcomes this classical limitation by increasing the depth of field by a factor of 100 in a single frame acquisition. Digital holograms are recorded by a CCD camera and processed to compute the complex amplitude of the light field involving the intensity and the phase of the signal. The Kirchhoff-

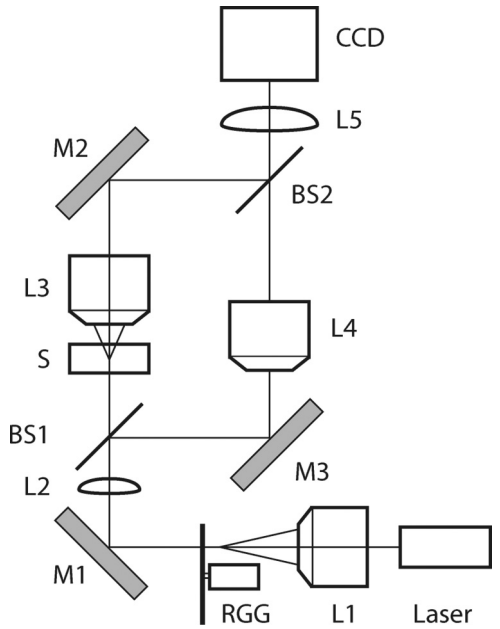


FIG. 1. Optical setup of the digital holographic microscope. L1: focusing lens; RGG: rotating ground glass for spatial coherence reduction; L2: collimating lens; L3, L4: identical microscope lenses (10×); L5: refocusing lens; CCD: charge-coupled device camera; M1–M3: mirrors; BS1, BS2: beam splitters; S: sample.

Fresnel propagation is then used to propagate the complex amplitude and to perform a digital holographic refocusing of the sample slide by slide. DHM is an elegant solution for three-dimensional tracking of small particles (Dubois *et al*. [29]) as it can easily provide their 3D position inside an experimental volume. Beyond the tracking of particles, DHM has been used in a wide variety of applications.

Different setups have been proposed in the literature to implement digital holography. We use a Mach-Zender interferometer (see Fig. 1) with microscope lenses (L3 and L4 with magnification 10 and NA 0.3) to provide the magnification. To decrease the coherent (speckle) noise inherent to coherent sources, we use a spatially reduced coherent source (Minetti *et al*. [30]). This source is obtained by focusing, with lens L1, an incident coherent beam (monomode laser diode, $\lambda =$ 635 nm) on a rotating diffuser (RGG). By adjusting the position of the diffuser on the optical axis, one can easily tune the spatial extent of the source and thereby control the spatial coherence of the light beam. The beam is then divided in two with a beam splitter (BS1). One beam passes through the experimental volume (object beam) and is recombined to the second beam (reference beam) by a second beam splitter (BS2) on the captor of the CCD camera. It has been shown by Dubois *et al*. [31] that the use of partially coherent illumination strongly increases the holograms' quality allowing the investigation in depth of a volume similar to a cube. The angle between the reference and the object beams is adjusted to create a thin fringe grating allowing implementation of the Fourier method (Kreis [32]). This method permits one to extract the complex amplitude from a single frame (hologram) acquired with a very short time (200 $\mu$s), indispensable for the monitoring of fast moving objects without blurring effects. Holograms of

1280 × 1024 pixels are captured at a frequency of 24 frames/s covering a field of view of 1057 × 846 $\mu$m (camera JAI CV-M4). The depth investigation is performed slide by slide in the range 0, –1000 $\mu$m (the focus plane of the microscope is placed on the bottom wall of the capillary; the propagation direction of light is considered as positive and the reconstruction direction negative). With this magnification, the precision on the position of an object in the $X$ and $Y$ directions is about 1 $\mu$m and about 20 $\mu$m in the $Z$ direction.

The $XY$ position of the moving particle is determined manually. The $Z$ position is performed automatically thanks to a best focus determination based on the minimum value of the integrated amplitude modulus as in Dubois *et al.* [33] (within a region of interest of 140 × 140 pixels around the particle). The $Z$ positions obtained are later checked by an operator. The procedure is repeated for a sequence of 600 holograms covering a period of time of 25 s.

The experimental setup comprises a DHM developed at the Microgravity Research Centre and a test sample made of a borosilicate glass tube. Differently from the previous works of one of the present authors, the glass tube has a square cross section with a dimension of 1 mm and a wall thickness of 0.2 mm. The square cross section is important in order to avoid optical distortion on a round tube as reported in Buffone *et al.* [3].

The liquid used is ethanol and the tracer particles are made of polystyrene latex with a diameter of 15.17 ± 0.14 $\mu$m. Only a few particles are put inside the ethanol as reported in Fig. 2; the meniscus interface is also marked in this figure.

In order to evaluate the influence of gravitational forces arising from the mismatch between tracers and fluid density, the following formula (coming from Stokes drag law) is used [24]:

$$U_{zP} - U_z = d_P^2 \frac{\rho_P - \rho}{18\mu} g,$$

where $U_{zP}$ and $U_z$ are the particle and fluid vertical velocity components, respectively, $d_P$ is the particle diameter, $\rho_P$ (1000 kg/m$^3$) and $\rho$ (789 kg/m$^3$) are the particles and fluid density, respectively, $\mu$ (0.001 095 Pa s) is the fluid dynamic viscosity, and $g$ is the gravitational acceleration. Applying the aforementioned formula to the present case, leads to

$$U_{zP} - U_z \cong 2.6 \times 10^{-5}\ \mathrm{m\,s^{-1}},$$

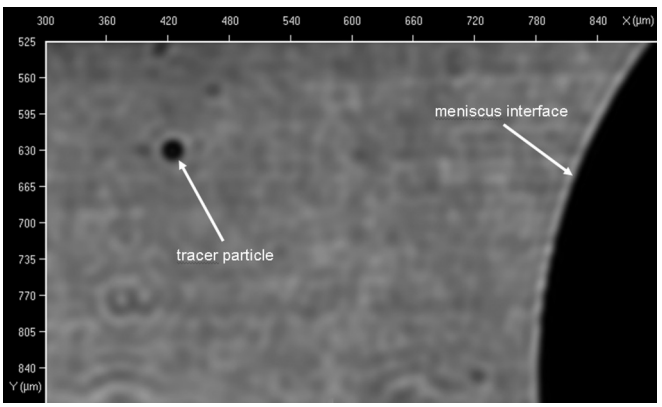


FIG. 2. Picture from digital holographic microscope showing part of the meniscus interface and the tracer particle.

whereas the particle's velocity measured along ($U_{zP} \cong 77 \times 10^{-5}$ m s$^{-1}$) the meniscus is higher. Therefore, we can assume the particles to behave as though they are neutrally buoyant.

Only half the tube width is considered and only one section of the 3D Marangoni vortex is unveiled. During different experiments conducted to have a single tracer particle, also the lower half of the tube cross section has been inspected and it has been found that the flow pattern is indeed oscillatory as in the upper half. In addition, a previous study by Buffone *et al.* [3] reported symmetrical flow pattern in horizontal optical sections with respect to the tube axis. The $Z$ axis of the holographic microscope starts on the bottom of the test tube and is directed as the gravity vector. For this reason the $Z$ coordinate reported in the following figures is always negative.

A limitation of the DHM for this application is the fact that when the tracer particle approaches the meniscus interface it disappears. This is due to the optical distortion of a 3D curved meniscus interface.

## III. RESULTS AND DISCUSSION

The present work is a study of self-induced thermocapillary convection inside the liquid phase of an evaporative meniscus of ethanol inside a 1-mm$^2$ borosilicate tube. The evaporation rate along the curved meniscus interface is not uniform, being larger at the meniscus wedge than in the middle (Buffone and Sefiane [25]); this creates differences in temperature which in turn generate gradients of surface tension which is the driving mechanism for the convection observed. The tube is positioned horizontally on the digital holographic microscope. Along the horizontal sections of the tube the surface tension driving force is symmetrical, whereas along the vertical sections there is a competition between surface tension and gravity forces which produces a nonsymmetrical driving force.

The objective of the present study is to follow a tracer particle and determine its 3D trajectory. With the DHM a tracer particle was tracked while it made several loops in the liquid phase next to the meniscus interface. Trajectories are reported in the following figures.

Figure 3 reports the 3D trajectory of the tracer particle as it completes one loop. In the inset on the top left corner a

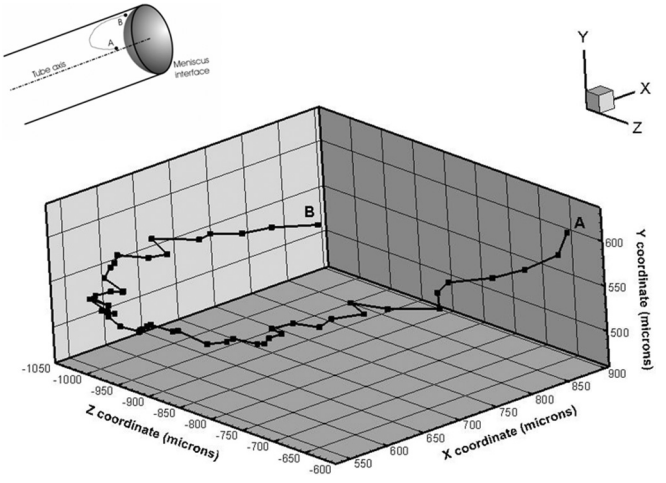


FIG. 3. Tracer particle 3D trajectory.

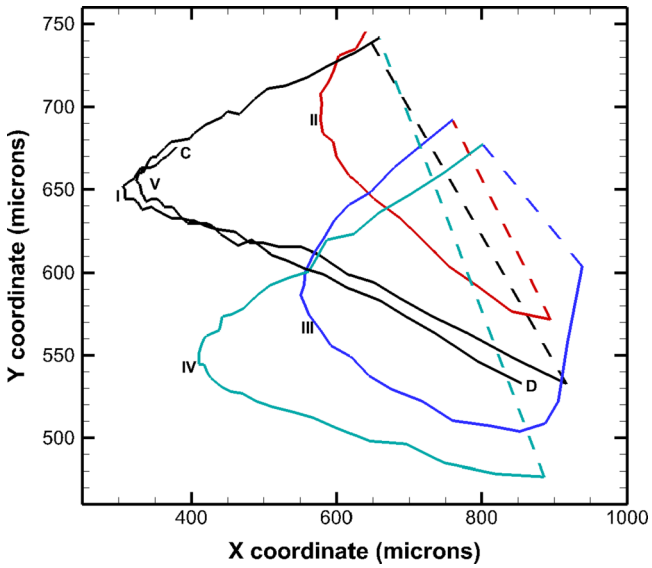


FIG. 4. (Color online) Tracer particle trajectory (2D projection).

schematic drawing shows the tube with its axis along the $X$ coordinate, the meniscus interface, and the particle trajectory. As can be seen from this figure the loop misses the part of the trajectory along the meniscus interface which is from **A** to **B**. As previously mentioned, this is due to the fact that the optical distortion due to the 3D curved meniscus interface does not allow tracing the particle along the meniscus. The small-scale fluctuations in the trajectory of Fig. 3 are intrinsic to the phenomenon being presented and are outside the accuracy of the DHM measurements. As shown by Fig. 3 there is an important displacement of the tracer in the $Z$ direction which is in excess of 600 microns. Therefore, we can say that the Marangoni convection is highly 3D.

Figure 4 reports the trajectory of the same tracer particle as it completes five loops starting from point **C** and finishing in point **D**. In this figure the dashed part of the trajectory is not real, because as it has been pointed out when the tracer particle is along the meniscus interface it cannot be tracked. As shown, the tracer particle makes loops of different dimensions and position. However, it is important to note that after four loops the tracer returns to the first loop. This can be seen in Fig. 4 with loops **I** and **V**.

The periodic oscillatory pattern also reported in a previous work (Buffone *et al*. [4]) is more clearly seen in Fig. 5, where $X$, $Y$, and $Z$ coordinates of the tracer particle are reported. In Buffone *et al*. [4] the meniscus position and two-dimensional (2D) $\mu$-PIV velocity maps were presented. In the present work the 3D nature of the Marangoni convection for an evaporative meniscus is finally and clearly unveiled.

From Fig. 5 it can be seen that the $X$, $Y$, and $Z$ coordinates of the tracer particle oscillate while the particle describes different loops of the Marangoni cell. Every four loops the particle returns to the first loop and therefore we can consider this phenomenon to be periodic with one cycle (between **L** and **M**) completing in around 8 s, which corresponds to a frequency of around 0.125 Hz. The total length of the DHM acquisition is 25 s, corresponding to over three complete oscillatory periods.

Following the dimensionless analysis reported by Buffone *et al*. [3] where the heat to sustain the evaporation comes from the surrounding environment of the tube, the following heat balance can be written:

$$mh_{fg} = 2\pi Rk_a \left\{ 0.6 + \frac{0.387[CR^3(T_a - T_w)]^{1/6}}{\left[1 + \left(\frac{0.559}{\mathrm{Pr}}\right)^{9/16}\right]^{8/27}} \right\}^2 \times (T_a - T_w),$$

where $k_a$ is the air thermal conductivity, $C$ is a constant incorporating air properties, $T_a$ is the ambient temperature, $T_w$ is the tube wall temperature, and Pr is the Prandtl number. We introduce the Reynolds number as

$$\mathrm{Re} = \frac{\mathrm{Ma}}{\mathrm{Pr}} = \frac{UR}{\nu},$$

where $U$ is the fluid velocity, $R$ is half the tube size, and $\nu$ the kinematic viscosity. From this latter equation the fluid characteristic velocity can be written as

$$U = \frac{\frac{\partial\sigma}{\partial T}\frac{\partial T}{\partial R}R}{\mu},$$

from which the characteristic frequency ($f^*$) is the reciprocal of the convection time scale ($\tau$) and can be written as

$$f^* = \frac{1}{\tau} = \frac{\frac{\partial\sigma}{\partial T}\frac{\partial T}{\partial R}}{\mu}.$$

The normalized frequency $\psi$ is derived by dividing the measured frequency (that corresponds to a single loop in Fig. 5 between **L** and **N** which is equivalent to almost 0.6 Hz) with the characteristic frequency ($f^*$) which gives

$$\psi = \frac{f}{f^*} = 0.016,$$

a value that is close (11% difference) to the normalized vorticity for ethanol and 1-mm tube diameter reported in Buffone *et al*. [3]. This low value of normalized frequency would be much higher if the temperature difference along the curved meniscus interface was measured.

Three runs have been analyzed with a new filled tube and new tracer particle. The oscillatory periodic phenomenon described in the present work has been observed in all three runs; the measured maximum deviation of the tracer particles in the three runs is less than 50 $\mu$m.

The dimensionless numbers describing the phenomenon presented in this work are Marangoni (Ma $= [(\partial\sigma/\partial T)(\partial T/\partial R)R^2]/\mu k$) and the Rayleigh numbers [Ra $= (g\beta\,\Delta T R^3)/\nu k$] along the Bond number [Bo $= (\rho g R^2)/\sigma$], where $\sigma$ is surface tension, $T$ temperature, $R$ tube dimension, $\mu$ dynamic viscosity, $\kappa$ thermal diffusivity, $g$ gravity, $\beta$ thermal expansion coefficient, $\nu$ kinematic viscosity, and $\rho$ density. For the present case with ethanol at 20 °C we have a surface tension of 0.022 N/m, a liquid density of 789 kg/m$^3$, and a characteristic dimension of 1 mm. The estimated Bond number for the present case is around 0.35. This means that despite the phenomenon being Marangoni driven, buoyancy effects are important and the competition between buoyancy and surface tension might well be responsible for the observed periodic motion of the tracer particle.

The oscillatory nature of the Marangoni flow studied is due, as also pointed out in Buffone *et al*. [4], to the competition

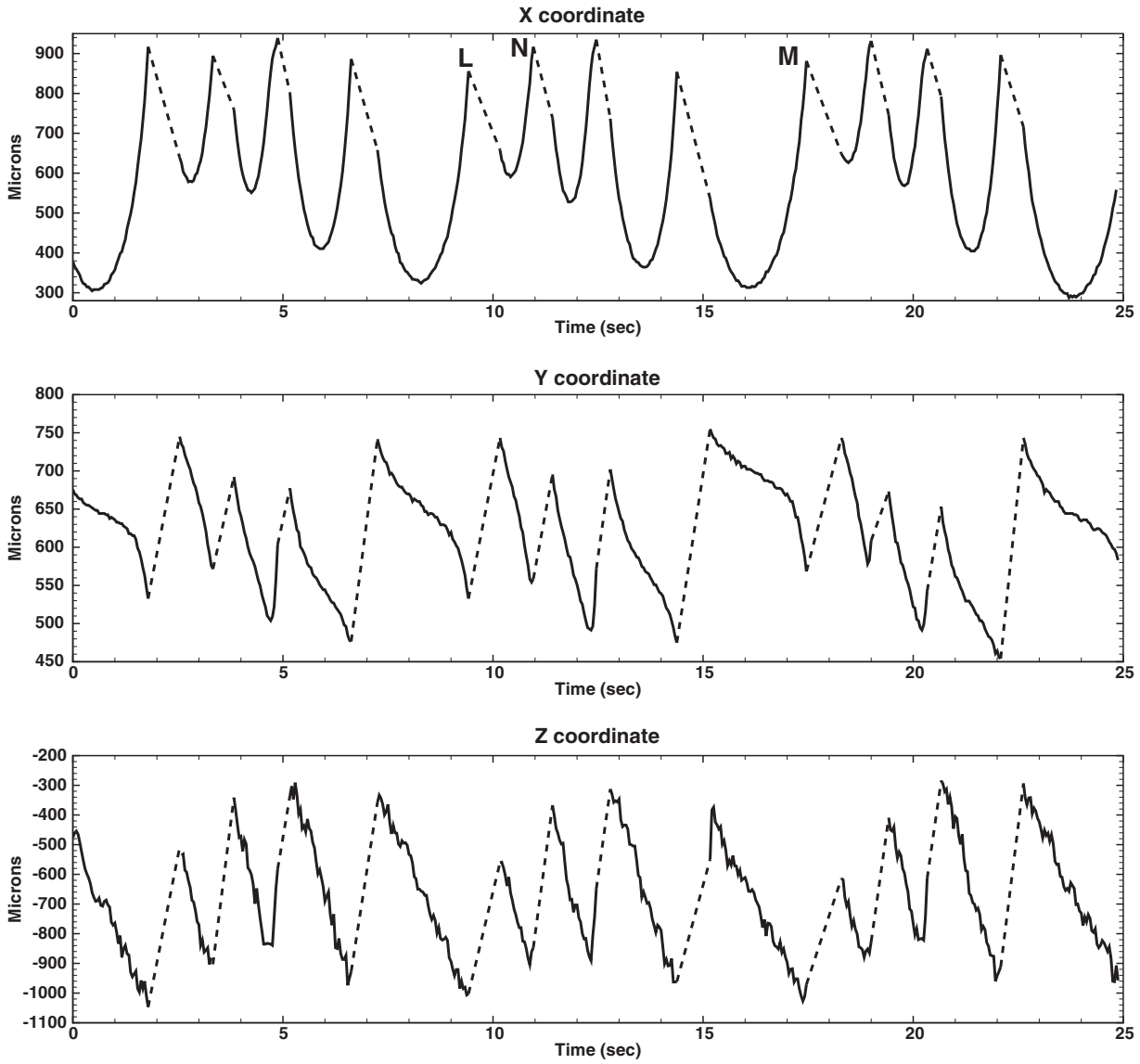


FIG. 5. $X$, $Y$, and $Z$ time evolution of the tracer particle position.

of surface tension and gravity forces. In Buffone *et al.* [4] the oscillations of the meniscus interface clearly caused oscillation in the Marangoni flow. No apparent oscillations of the meniscus interface were observed in the present investigation.

A lot of work has been done in the past on liquid bridges, and oscillatory flow patterns have been reported for both low and high Prandtl numbers. These oscillatory flows in liquid bridges have been reported as early as the 1980s as in Schwabe and Scharmann [34] and Wang *et al.* [35] for high Prandtl numbers ($\sim$10), where the cause of oscillation has been attributed to the competition of thermocapillary and buoyancy; the critical Marangoni number in these two studies was around $10^4$. In another numerical study by Yao *et al.* [36] for low Prandtl numbers ($10^{-2}$), for increasing Marangoni number between 15 and 75, the flow mutated from steady axisymmetric to three-dimensional steady and then eventually three-dimensional oscillatory flow.

More in-depth study is necessary to better understand this interesting instability phenomenon, especially with measurements of interfacial temperatures. It is highly likely that hydrothermal waves are present.

## IV. CONCLUSIONS

A digital holographic microscope has been used to trace the 3D motion of a tracer particle in an evaporating meniscus of ethanol inside a square borosilicate glass with a dimension of 1 mm. The tube was placed horizontally and the meniscus was positioned at the tube mouth. The periodic oscillatory nature of the Marangoni convection as previously reported in Buffone *et al.* [4] was confirmed in the present work. In addition, in this work the 3D trajectory of the tracer particle has been clearly reported and discussed. The trajectory is found to be periodic with a characteristic frequency of 0.125 Hz. The periodic oscillatory nature of the Marangoni convection is due to the competition of surface tension and gravity forces.

[1] V. G. Levich and V. S. Krylov, Annu. Rev. Fluid Mech. **1**, 293 (1969).
[2] R. K. Zeytounian, Int. J. Eng. Sci. **35**, 455 (1997).
[3] C. Buffone, K. Sefiane, and J. R. Christy, Phys. Fluids **17**, 052104 (2005).
[4] C. Buffone, K. Sefiane, and W. Easson, Phys. Rev. E **71**, 056302 (2005).
[5] J. R. A. Pearson, J. Fluid Mech. **4**, 489 (1958).
[6] L. E. Scriven and C. V. Sternling, Nature **187**, 186 (1960).
[7] H. Wang, J. Y. Murthy, and S. V. Garimella, Int. J. Heat Mass Transfer **51**, 3007 (2008).
[8] M. L. Potash and P. C. Wayner, in *Proceedings of AIChE 63rd Annual General Meeting, Chicago*, 1970.
[9] M. L. Potash and P. C. Wayner, NTIS Report No. RPI TCTP-001, NTIS PB-235 (1974).
[10] G. Preiss and P. C. Wayner, J. Heat Transfer **96**, 178 (1976).
[11] P. C. Wayner, Y. K. Kao, and L. V. LaCroix, Int. J. Heat Mass Transfer **19**, 487 (1976).
[12] A. Mirzamoghadam and I. Catton, J. Heat Transfer **110**, 201 (1988).
[13] L. W. Swanson and G. C. Herdt, J. Heat Transfer **114**, 434 (1992).
[14] S. DasGupta, J. A. Schonberg, and P. C. Wayner, J. Heat Transfer **115**, 201 (1993).
[15] P. C. Wayner, J. Heat Transfer **116**, 938 (1994).
[16] R. Reyes and P. C. Wayner, J. Heat Transfer **118**, 822 (1996).
[17] D. Khrustalev and A. Faghri, J. Heat Transfer **117**, 740 (1995).
[18] J. A. Schonberg, S. Das Gupta, and P. C. Wayner, Exp. Therm. Fluid Sci. **10**, 163 (1995).
[19] V. Sartre, M. C. Zaghdordi, and M. Lallemand, Int. J. Therm. Sci. **39**, 498 (2000).
[20] C. Hohmann and P. Stephan, Exp. Therm. Fluid Sci. **26**, 157 (2002).
[21] C. Buffone and K. Sefiane, Exp. Fluids **39**, 99 (2005).
[22] C. Buffone and K. Sefiane, Int. J. Multiphase Flow **30**, 1071 (2004).
[23] C. Buffone and K. Sefiane, Int. J. Multiphase Flow **32**, 1287 (2008).
[24] R. Markus, C. Willert, and J. Kompenhans, *Particle Image Velocimetry: A Practical Guide* (Springer, London, 1998).
[25] C. Buffone and K. Sefiane, Exp. Therm. Fluid Sci. **29**, 65 (2004).
[26] D. Schwabe, Physicochem. Hydrodyn. **2**, 263 (1981).
[27] P. Chamarthy, H. K. Dhavaleswarapu, S. V. Garimella, J. Y. Murthy, and S. T. Wereley, Exp. Fluids **44**, 431 (2008).
[28] Z. Pan, F. Wang, and H. Wang, Microfluid. Nanofluid. **11**, 327, (2011).
[29] F. Dubois, N. Callens, C. Yourassowsky, M. Hoyos, P. Kurowsky, and O. Monnom, Appl. Opt. **45**, 864 (2006).
[30] C. Minetti, N. Callens, G. Coupier, T. Podgorski, and F. Dubois, Appl. Opt. **47**, 5305 (2008).
[31] F. Dubois, M.-L. Novella Requena, C. Minetti, O. Monnom, and E. Istasse, Appl. Opt. **43**, 1131 (2004).
[32] T. Kreis, J. Opt. Soc. Am. A **3**, 847 (1986).
[33] F. Dubois, C. Schockaert, N. Callens, and C. Yourassowsky, Opt. Express **14**, 5895 (2006).
[34] D. Schwabe and A. Scharmann, Adv. Space Res. **3**, 89 (1983).
[35] A. Wang, Y. Kamotani, and S. Yoda, Int. J. Heat Mass Transfer **50**, 4195 (2007).
[36] L. Yao, Z. Zeng, X. Li, J. Chen, Y. Zhang, H. Mizuseki, and Y. Kawazoe, J. Cryst. Growth **316**, 177 (2011).